JOURNAL OF PROPULSION AND POWER
Vol. 17, No. 3, May–June 2001

Sidewall Interaction in an Asymmetric Simulated Scramjet Inlet Configuration

D. V. Gaitonde,* M. R. Visbal,† and J. S. Shang‡
Air Vehicles Directorate, Air Force Research Laboratory, Wright–Patterson Air Force Base, Ohio 45433-7521
and
A. A. Zheltovodov§ and A. I. Maksimov¶
Institute of Theoretical and Applied Mechanics, 630090 Novosibirsk, Russia

The complex three-dimensional flowfield arising from the interaction of a shock-induced turbulent vortical structure with a sidewall boundary layer is examined by numerically solving the Reynolds-averaged compressible Navier–Stokes equations closed with a two-equation k–ϵ turbulence model. The configuration considered is representative of a scramjet inlet compression system and comprises two opposed sharp fins mounted on a flat plate at 7 and 15 deg to the incoming flow. The flowfield arising from the impingement of a primary vortical structure on the 7 deg fin is found to be strongly dependent on the state of the boundary layer on this sidewall. An elegant turbulent kinetic energy production-limiting technique is employed to reproduce the complicated saddle-spiral topology observed in the experimental sidewall oil flow pattern. Detailed analysis of the computed flowfield shows that the main consequence of the interaction is characterized by the ejection of the vortex formed at the fin–plate junction (corner vortex in the terminology of single-fin flows) in a direction along the sidewall and normal to the plate. The flowfield asymptotes to the classic two-dimensional shock–turbulent boundary-layer interaction at large distances from the plate.

Nomenclature

C	=	saddle point
EXP	=	expansion
F	=	focus
IL	=	number of points in streamwise direction
JL	=	number of points in plate-normal direction
KL	=	number of points in spanwise direction
k	=	turbulent kinetic energy
P_k	=	production of turbulent kinetic energy
P_t	=	total pressure
p	=	static pressure
R	=	line of attachment (divergence)
Re	=	Reynolds number
S	=	line of separation (coalescence)
T	=	temperature
TKE	=	turbulent kinetic energy, k
u_i	=	Cartesian velocity
X	=	streamwise distance normalized by boundary-layer height ($X = x/\delta$)
x	=	streamwise coordinate
y	=	plate-normal coordinate
z	=	spanwise (cross-flow) coordinate
γ	=	turbulent kinetic energy production-limiting coefficient
δ	=	height of incoming boundary layer
δ_{ij}	=	Kronecker delta function
ϵ	=	dissipation of turbulent kinetic energy
θ	=	momentum thickness of incoming boundary layer
μ_t	=	eddy viscosity
ξ_i	=	computational coordinate
ρ	=	density
$\tau_{t_{ij}}$	=	turbulent shear stress tensor

Subscripts

L	=	component of shock system due to left fin (looking downstream)
R	=	component of shock system due to right fin (looking downstream)
w	=	wall
∞	=	freestream

Received 22 February 2000; revision received 28 September 2000; accepted for publication 21 November 2000. This material is declared a work of the U.S. Government and is not subject to copyright protection in the United States.

*Senior Research Aerospace Engineer, Building 146, Room 225, 2210 Eighth Street; datta@vaa.wpafb.af.mil. Associate Fellow AIAA.
†Technical Area Leader, VAAC, 2210 Eighth Street. Associate Fellow AIAA.
‡Senior Scientist, VAA, 2210 Eighth Street. Fellow AIAA.
§Senior Research Scientist, Institute of Theoretical and Applied Mechanics, Institutskaya Street. Member AIAA.
¶Senior Research Scientist, Institute of Theoretical and Applied Mechanics, Institutskaya Street, 4/1.

Introduction

THE effort to achieve sustained hypersonic flight and rapid access-to-space has generated a resurgence of interest in the design and development of scramjet propulsion. Several outstanding problems will need to be resolved, however, before a mature design can be proposed. These complications arise from the need to obtain efficient and rapid mixing and combustion to yield acceptable thrust levels. Among the principal phenomena that determine the details of the flowfield in proposed scramjet designs are shock wave–turbulent boundary-layer interactions. The shock waves arise from geometric features introduced to achieve some degree of flow compression, whereas boundary layers arise naturally on adjacent surfaces. Such interactions cause significant degradation in the quality of the flowfield as measured through distortion and pressure recovery levels.[1,2] Observed features include boundary-layer separation and the appearance of various vortical structures.

The geometry examined in this work is shown in Fig. 1 and consists of two fins mounted asymmetrically on a flat plate. The flow and geometric parameters are chosen to reproduce the experimental results of Zheltovodov et al.[3] Looking downstream, the left and right fins are positioned on a flat plate at angles of attack of 7 and 15 deg, respectively. Shocks emanating from the two fins form a crossing pattern (hence, the term *crossing-shock configuration*) and interact with the plate boundary layer. In short form, the interaction produced will be denoted by specifying the two fin angles: this is thus the 7×15 deg interaction. The incoming flow is at Mach 4, the

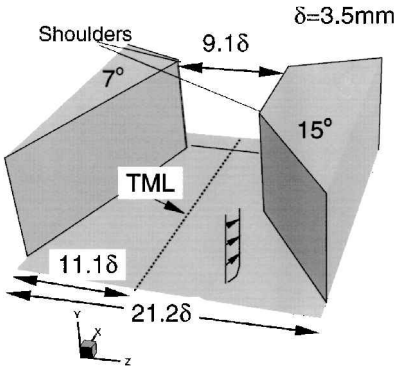

Fig. 1 Geometry of crossing-shock configuration. TML = throat middle line.

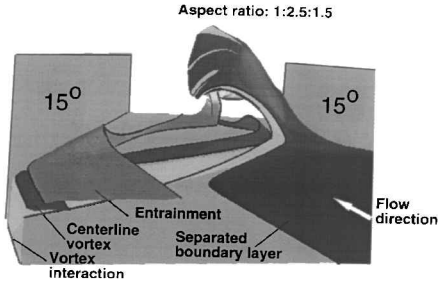

Fig. 2 Flow regimes observed in 15 × 15 deg interaction, as depicted with stream surfaces (from Ref. 5).

Reynolds number is 87.5×10^6 per meter, and the total pressure, P_t, is 1.5×10^6 Pa. The equilibrium plate boundary-layer momentum thickness at the leading edges of the fins is measured at 0.13 mm.

The description of a separated three-dimensional flowfield structure is necessarily complex. In a previous sequence of joint computational–experimental papers,[4–6] the dominant features of the mean flowfield arising in double-fin interactions were described by defining various regimes through their correlation with the surface oil flow pattern. Four principal regimes are employed in this description: separated boundary layer, vortex interaction, centerline vortices, and entrainment. For a symmetric 15 × 15 deg interaction, these features are exhibited in Fig. 2, which has been taken from Ref. 5. Note that to highlight the regimes, an artificial aspect ratio has been applied. The separated boundary layer does not reattach but rather arches downstream in a manner that permits fluid from the other regimes to sweep spanwise from near the corners and to occupy the region beneath. The vortex interaction flow forms a shear layer with the separated boundary layer, and the entrainment regime brings high-energy fluid near the plate through an impingement process that occurs near the fin–plate corner. This fluid subsequently expands in the spanwise direction and, in strong interactions, a wall-jet-like structure is obtained. Near the center of the channel, this regime separates to yield the last feature: a pair of secondary vortices (symmetric in this case) straddling the symmetry plane. This description of the interaction of the shocks with the boundary layer developing on the plate will be termed the "primary" interaction to distinguish it from sidewall interaction to be described later. Similarly, the term "primary" vortical structure will be employed to refer to the combination of all these regimes, with the exception of the centerline vortices.

The present paper is concerned with the highly asymmetric 7 × 15 deg interaction. In Ref. 6, it was shown that the same four features described above for symmetric interactions are identifiable in asymmetric ones. The separated boundary-layer regime in this asymmetric flowfield is shown in Fig. 3 with some of the prominent lines of coalescence (S_1, S_2, and S_{12}) observed in the simulated plate oil flow pattern. Naturally, symmetry about the channel centerline is lost. On the strong (15 deg) interaction side, the separation surface emanating from the line of separation S_2 is very steep and rolls up into a clearly discernible vortical motion. This primary structure

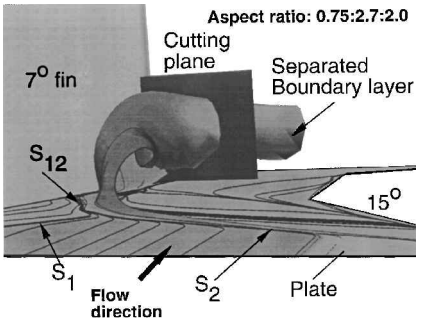

Fig. 3 Separated boundary-layer regime in 7 × 15 deg interaction with select lines of simulated plate oil flow pattern. Cutting plane illustrates the curvature of the separation surface.

arising out of the separation of the incoming plate boundary layer is then swept toward the 7 deg fin (weak interaction side), where it then impacts on the sidewall boundary layer in a complex fashion to cause significant sidewall loading. The purpose of the present paper is to establish a clear understanding of the resulting flowfield, with specific emphasis on elucidating the streamline and shock structure.

The theoretical model and numerical method are first briefly described. Various aspects of computational and experimental observations are then compared. Next, discrepancies observed with the baseline turbulence model are addressed by incorporating a carefully chosen modification designed to simulate the proper state of the sidewall boundary layer and thus to reproduce the experimental data to adequate accuracy. Finally, the computed flowfield is mined to extract the coherent features of the sidewall interaction, which are then correlated with the shock pattern.

Theoretical Model

The mean flow field is assumed to be described by the full three-dimensional Reynolds-averaged compressible Navier–Stokes equations written in strong conservation form and mass-averaged variables.[7] The inviscid fluxes are evaluated to nominal third-order accuracy with the characteristic-based Roe scheme.[8] Viscous terms are evaluated to second-order accuracy through a centered approach. The turbulent Prandtl number is assumed to be constant ($Pr_t = 0.9$), and Sutherland's law is employed to evaluate the molecular viscosity. The baseline turbulence model is a variant of the original two-equation k–ϵ[9,10] formulation, modified to include a compressibility correction.[11] These standard components of the algorithm have been described extensively elsewhere[12–14] and are not repeated here. However, pertinent elements of the turbulence model are reproduced later in the context of modifications employed to control the state of the sidewall boundary layer. A detailed comparison of the performance of various turbulence models may be found in the documentation of Ref. 15.

An extensive mesh resolution study has been performed for these interactions at a wide range of interaction strengths and Mach numbers. These results are presented in Refs. 4, 5, and 16. For completeness, Fig. 4, taken from Ref. 17, shows surface pressure along the centerline for a 15 × 15 deg configuration and the same flowfield parameters in the present work. The two meshes referred to in the figure are composed of 9.9×10^5 and 1.9×10^6 points, respectively, and discretize the domain on only one side of the plane of symmetry. Even though the present 7 × 15 deg interaction is weaker, and thus is anticipated to yield weaker gradients, the density of the mesh employed is approximately the same as of the first of the two meshes of Fig. 4. The final grid consists of $123 \times 88 \times 197 = 2.1 \times 10^6$ points in the streamwise (x), plate-normal (y), and spanwise (z) directions, respectively. The mesh spans the entire region between the fins because this configuration is not symmetric. The spacing near the wall in the y direction is adjusted so that, in the incoming boundary layer, the first point is at 0.7 wall units from the surface.

The boundary conditions are similar to those employed in previous similar studies.[5] On solid surfaces, the no-slip condition is enforced, the wall temperature is specified to match the experimental observation ($T_w = 270$ K), and the normal pressure gradient, k

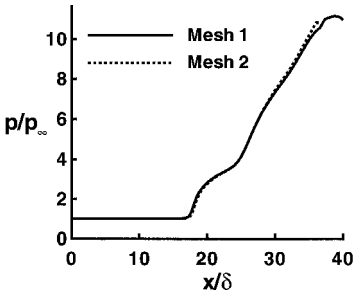

Fig. 4 Centerline pressure obtained with two meshes in 15 × 15 deg interaction. Mesh 1 has 9.9×10^5 points, mesh 2 has 1.9×10^6 points.

and ϵ, are all assumed to be zero. The incoming boundary-layer profile is specified at a distance of 4δ ($\delta = 3.5$ mm) upstream of the fin leading edges by matching the momentum thickness ($\theta = 0.13$ mm at the fin leading edge with separate two-dimensional calculations. The downstream and top boundaries are assumed to be far enough away for the application of simple zero-gradient extrapolation of all quantities.

Results

Validation

As noted earlier, the primary objective of this work is to describe the flowfield structure of the sidewall interaction. The structure of the sidewall interaction, as obtained in experiment, is principally determined from observation of the oil flow pattern on the sidewall. These data are now employed to evaluate and improve the fidelity of the solution procedure. The sidewall oil flow pattern obtained from the computation with the baseline model is exhibited in Fig. 5 with the experimental inference. Note that the expression "oil flow pattern," when employed in the context of computations, denotes the method of simulating the equivalent of experimental oil flow observations by releasing particles at the first mesh point away from the surface and following their trajectory under the assumption that the plate-normal velocity is zero. An equivalent method of utilizing the surface skin-friction vector yields nearly identical results. The fin leading edge constitutes the extreme left of the region plotted, and the lower edge of the domain is the corner formed at the juncture of the plate and the fin. The two parts of Fig. 5 are only approximately to the same scale because small artificial aspect ratios are introduced when sketching the experimental inference. In the region where the separated vortical structure of Fig. 3 impinges on the sidewall, the interaction is characterized by an upstream line of coalescence (S_5) and a downstream line of divergence (R_5). For simplicity, the notation of the experimentalists[3] is followed. These two lines are classic indicators of separation followed by attachment in two-dimensional situations under the influence of severe adverse-pressure gradients as occur, for example, in compression corners.[18] It is shown later, however, that in the present three-dimensional interaction, the two-dimensional situation is not recovered because fluid separating at S_5 does not attach at R_5.

In comparing experimental data with computations, it is evident that the streamwise distance between the two lines is considerably shorter in the latter. Significant discrepancies are also apparent near the fin–plate corner. This deficiency of the computational results is best described by reference to the observed critical points, that is, points where the shear stress is zero. The phenomenological significance and mathematical properties of such points have been described extensively in the literature.[19,20] The experimental pattern exhibits a saddle (C_2) and focus (F_1) combination that is conspicuously absent in the computations. The computational deficiency is significant because a focus such as the one observed in the experiment indicates the origin of a vortex filament entering the flow under off-design conditions. The potential interaction of this feature with downstream components in a scramjet must be considered as an additional complication. Note further that although both patterns exhibit a vertical orientation of oil flow lines away from the corner, only the experimental inference has a region beneath C_2 where the surface streamlines actually move downward, that is, toward the corner. Finally, the experimental line S_5 curves streamwise near the outer

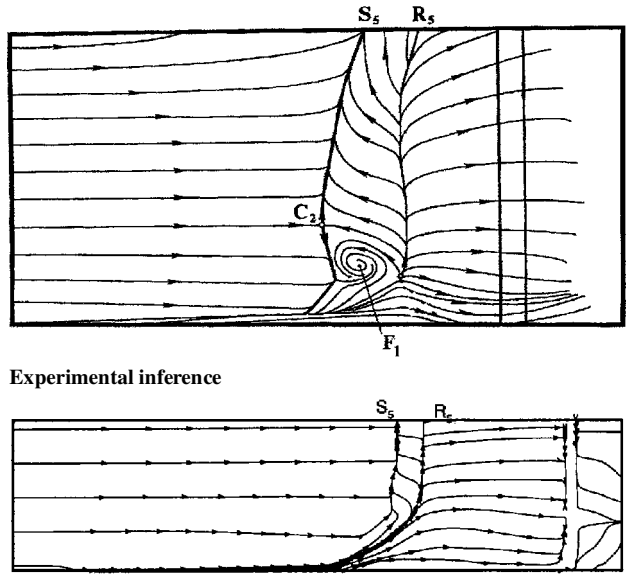

Fig. 5 Comparison of sidewall surface oil flow pattern on 7 deg fin. *C* = saddle point, *F* = focus, *S* = separation, *R* = attachment.

edge of the fin because of its finite height in the experiment. No such curvature is evident in the computation as a result of the conditions applied at the top boundary, which effectively assume a sidewall of infinite vertical extent. This discrepancy may therefore be dismissed as an end effect of relatively little significance in the present study.

A possible explanation for the topological and interaction size discrepancies is based on the state of the sidewall boundary layer in the region of vortical structure impingement. In the simulation, the sidewall boundary layer becomes turbulent forthwith at the fin leading edge, a situation that may not reflect the actual experiment. This hypothesis may be explored in several ways. Potentially, the most accurate method would require a direct numerical simulation. However, at present, such methods are not feasible, not only because computational resource demands exceed availability, but also, because transition needs to be simulated, far more precise information about wind tunnel conditions, such as freestream turbulence and noise levels, is also required. We choose the following heuristic approach to evaluate the effect of the state of the fin boundary layer on the properties of the sidewall interaction.

The procedure, based on limiting the production of turbulent kinetic energy, was proposed by Menter[21] in the context of the k–ω model to prevent the unphysical buildup of eddy viscosity. In the present work, this technique is employed to control the development of the sidewall boundary layer. The implementation requires modification of the term dictating production of turbulent kinetic energy, P_k, in the k–ϵ model:

$$P_k = \frac{1}{Re}\tau_{t_{ij}}\frac{\partial \xi_k}{\partial x_j}\frac{\partial u_i}{\partial \xi_k} \tag{1}$$

where

$$\tau_{t_{ij}} = \mu_t\left(\frac{\partial \xi_k}{\partial x_j}\frac{\partial u_i}{\partial \xi_k} + \frac{\partial \xi_k}{\partial x_i}\frac{\partial u_j}{\partial \xi_k} - \frac{2}{3}\delta_{ij}\frac{\partial \xi_l}{\partial x_k}\frac{\partial u_k}{\partial \xi_l}\right) \tag{2}$$

is the shear stress tensor, $\partial \xi_k / \partial x_j$ denote coordinate metrics, and u_i are Cartesian components of velocity. This term assumes very large values in the fin leading-edge shock, even in regions far removed from the plate, and triggers a rapid, almost immediate transition of the fin boundary layer. The procedure of Menter[21] consists of replacing P_k globally by P'_k where, with ρ and ϵ denoting the density and turbulence-energy dissipation term, respectively,

$$P'_k = \min(P_k, \gamma\rho\epsilon) \tag{3}$$

The value of γ is dependent on the flowfield under consideration. The value for γ employed by Menter for subsonic flows, $\gamma = 20$,

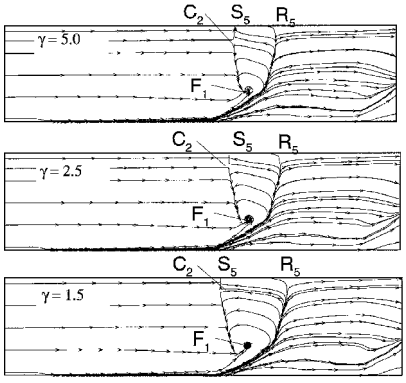

Fig. 6 Effect of limiting of turbulence energy production on the prediction of sidewall surface pattern with various values of γ.

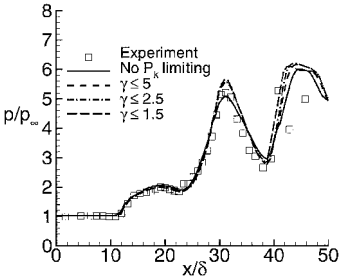

Fig. 7 Impact of turbulence energy production limiting on surface pressure along TML.

is not effective for the present case. To obtain an estimate of what levels of γ may be effective, it is noted that the peak value of $P_k/\rho\epsilon$ in the upstream equilibrium boundary-layer profile is 1.2, which sets the minimum value of γ because lower values than this affect the upstream incoming boundary-layer profile, thus altering momentum thickness and the features of the primary interaction. On the other hand, the largest value of P_k anywhere in the computed solution with the baseline model is 10.2, which sets a maximum level for γ. Thus, values of 5, 2.5, and 1.5 were examined.

The impact of this modification on the sidewall surface pattern with the three values of γ is depicted in Fig. 6. It is apparent that at $\gamma = 5.0$, there is a drastic improvement in the comparison with the experiment. Note particularly the increased reversed flow region between S_5 and R_5 and the appearance of the focus–saddle combination, $F_1 - C_2$, which satisfies the local rules of topological bifurcation. Reducing γ to 2.5 and then to 1.5 yields an increase in the size of the reversed flow region but has no additional topological impact.

It is natural to enquire whether the modification has affected other aspects of the interaction, such as the pressure and simulated oil flow patterns on the plate. This question is investigated in Figs. 7 and 8. In the former, the experimental surface pressure on the throat middle line (TML) is plotted with the computed results from the original and modified turbulence models. The abscissa and ordinate are normalized by the upstream boundary-layer thickness and the upstream static pressure, respectively. The figure indicates that the surface pressure is not affected in the major portion of the primary interaction. However, some variation is observed in the region of peak pressure, $X \sim 30$, where the computed results straddle the experimental values. Most of this change occurs when γ is lowered to 5, but further reduction has no impact.

The experimentally inferred oil flow pattern on the plate is exhibited in Fig. 8 with computed results with the unmodified and modified ($\gamma = 1.5$) turbulence models. Some of the major lines of coalescence and divergence are marked in each figure. It is evident that both computations reproduce the experimental results. Thus, the modifications to the turbulence model affect primarily the sidewall boundary layer and its interaction with the primary vortical structure. Before we proceed to elucidating the details of this sidewall interaction, note that a detailed discussion of the significance of each of the prominent features observed in Fig. 8 and the correlation with

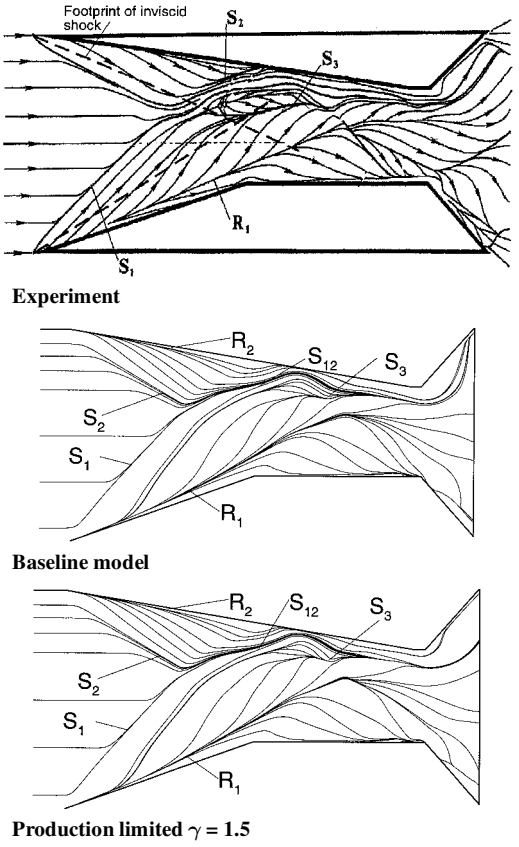

Fig. 8 Impact of turbulence energy production limiting on simulated oil flow pattern on plate.

the flowfield model of Fig. 3 has been provided in Ref. 6. Briefly, primary separation occurs at the lines of coalescence denoted S_1 and S_2, and primary attachment occurs at the lines of divergence R_1 and R_2, which form near the sidewalls. S_1 and S_2 merge downstream to form S_{12}, and a new line of attachment, denoted R_3, also appears. Two items of particular significance in this work are the corner vortices formed between the lines of divergence R_1 and R_2 and the corresponding fin–plate junction. These vortices have been generally ignored in previous crossing-shock interactions because of their relative unimportance in determining the dominant features of the main vortical structure. As demonstrated later, however, these vortices play an important role in the sidewall interaction.

Structure of Sidewall Interaction

The improved prediction of the sidewall–shock-vortex interaction permits an investigation of the details of the flowfield. The mean flowfield is elucidated first in terms of the streamline structure. Subsequently, the three-dimensional shock pattern is integrated into the description.

The principal elements of the interaction are presented in Fig. 9. The fin boundary layer separates at S_5: the associated surface of separation is identified as surface 1. Note that although this surface approaches the sidewall downstream of the line of attachment, R_5, it does not reattach. Reattachment is generally not observed when three-dimensional effects are present. Rather, fluid attaching at R_5 originates near the fin–plate corner. A truncated version of this regime is depicted as surface 2. This fluid originates outside of the corner vortex described later and, after attachment beneath surface 1 (at R_5), spans the entire region downstream of R_5.

As noted earlier, the sidewall interaction yields a focus–saddle ($F_1 - C_2$) combination (see Fig. 6). Further probing of the computed field reveals the liftoff of a vortex from the focus F_1. There are several possible sources of the vorticity observed in this vortex, which is distinct from and coexists with the primary structure described in Fig. 3. The principal sources of vorticity are the solid boundaries

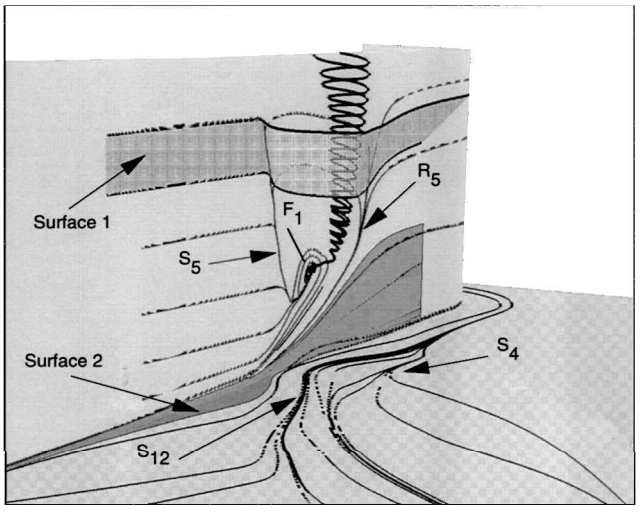

Fig. 9 Principal elements of sidewall interaction.

and curved shocks. Reference 6 contains a detailed discussion of the vorticity dynamics of the primary interaction. The fluid in this sidewall vortical structure is observed to originate from near the juncture formed by the fin and the plate, where, in this and similar interactions,[22] a small (relative to the large vortical structure of Fig. 3) corner vortex is present. This fluid first moves along the sidewall and away from the plate and is then ejected at F_1 in a spiral motion. The ejected structure is not transported downstream; rather, it traverses vertically away from the plate. At large distances from the plate, the two-dimensional asymptote is obtained as a result of separation caused by shock impingement on the fin boundary layer.

Shock Structure

As may be expected, there is a close correlation between the establishment of the mean streamline structure of the sidewall interaction and the associated three-dimensional shock-wave pattern. The structure of the shock-wave pattern is typically described through its trace on various planes. Previous efforts have employed this strategy to validate computational efforts[5] by direct comparison with planar laser scattering observations.[23] These efforts have proven the ability of the present high-resolution computational method to reproduce the observed experimental shock structure. The shock pattern observed in the present 7×15 deg interaction has been extensively described in Ref. 6. Although the prominent features remain unaffected, the shock structure is altered in the vicinity of the sidewall interaction primarily as a result of the change in size of the sidewall interaction, as summarized later.

In discussing the shock structure, the various elements of the shock system are distinguished with numerical labels, and where possible, suffixes L and R are appended for shocks that can be clearly ascribed to being caused by the 7 or 15 deg fins, respectively. For consistency, the notation closely follows that of Ref. 6, and pertinent items are reproduced in Table 1. Absent items represent features not relevant to the present description of the sidewall interaction. The shock structure at the upper boundary of the computed domain using the baseline (a) and the TKE limited model (b) is depicted in Fig. 10. The quantity plotted is the magnitude of the pressure gradient. Following the notation of Table 1, the primary inviscid shocks 3_L and 3_R intersect to yield the secondary inviscid shocks 9_L and 9_R.

Away from the corner formed by the fin and plate, the effect of the impingement of 9_R on the sidewall boundary layer is similar in some respects to that observed in two-dimensional situations (see, for example, Ref. 24). However, the details are strongly dependent upon the three-dimensionality of the flow near the fin–plate corner and due to expansions emanating from the shoulder of the opposing 15 deg fin. As shown in Fig. 10b, the interaction may be described in terms of a sidewall boundary-layer separation shock (18) with an expansion (EXP) and a recompression shock (19). The impact of the

Table 1 Notation in shock structure depiction

Description	Notation[a]
Primary rear shock	2
Primary inviscid shock	3
Secondary separation shock	6
Secondary rear shock	8
Secondary inviscid shock	9
Wall-jet shock	12
Tertiary separation shock	15
Tertiary inviscid shock	17
Sidewall boundary-layer separation shock	18
EXP	Expansion
Sidewall boundary-layer recompression shock	19

[a]Subscripts L and R indicate elements associated with left and right fins (looking downstream), respectively.

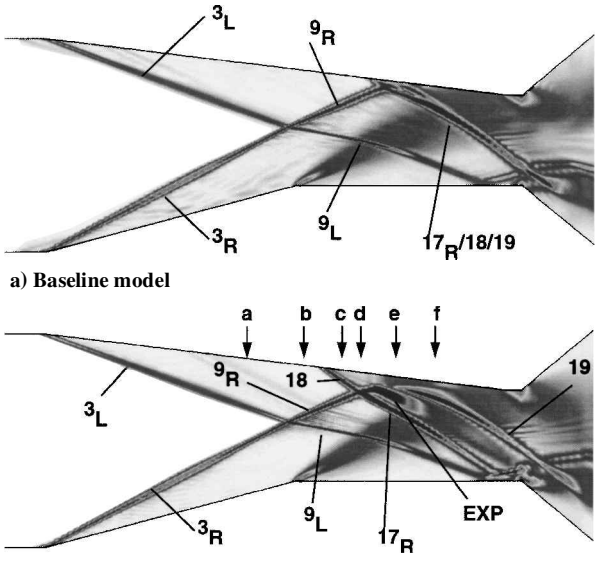

Fig. 10 Shock structure at top boundary of computed domain. Planform view.

turbulence model modification is clearly significant. The sidewall separation and recompression shocks are not well formed in the computations with the baseline model. This is attributable to the relatively small region of sidewall boundary-layer separation and the absence of strong three-dimensionality due to a well-defined ejected corner vortex. Consequently, with the original turbulence model, the shocks designated 17_R, 18, and 19 merge into a single entity at only short distances downstream of the sidewall interaction. This combined entity then interacts with the expansion emanating from the shoulder of the 15 deg fin.

The interdependence of the shock and streamline structure in the corner region is shown in Fig. 11 by plotting the shock structure on successive cross-flow planes. The location of these planes has been marked in Fig. 10b. The case where the separation shock of the R system, 6_R, has crossed the inviscid shock of the L system, 3_L, is shown in Fig. 11a. As the cutting plane is moved downstream, Fig. 11b, the separation shock imposes a severe adverse gradient on the corner vortex, consistent with the upward inclination of sidewall oil flow lines in Fig. 6 exhibit an upward inclination because of this interaction. The traces of two shocks are evident in regions away from the fin–plate corner, as shown in Fig. 11c. These are both to be considered as components of the same system in the sense that the relatively strong sidewall boundary-layer separation shock, 18, simply represents the upstream effect of the interaction of the inviscid secondary shock due to the R system, 6_R. The secondary separation shock, 6_R, reflects from the sidewall in a regular fashion and is designated the tertiary separation shock, 15_R. The pattern at the junction of several shocks, including 18, 9_R, and 17_R, which is the tertiary inviscid shock due to the R system, is shown in Fig. 11d. Near the

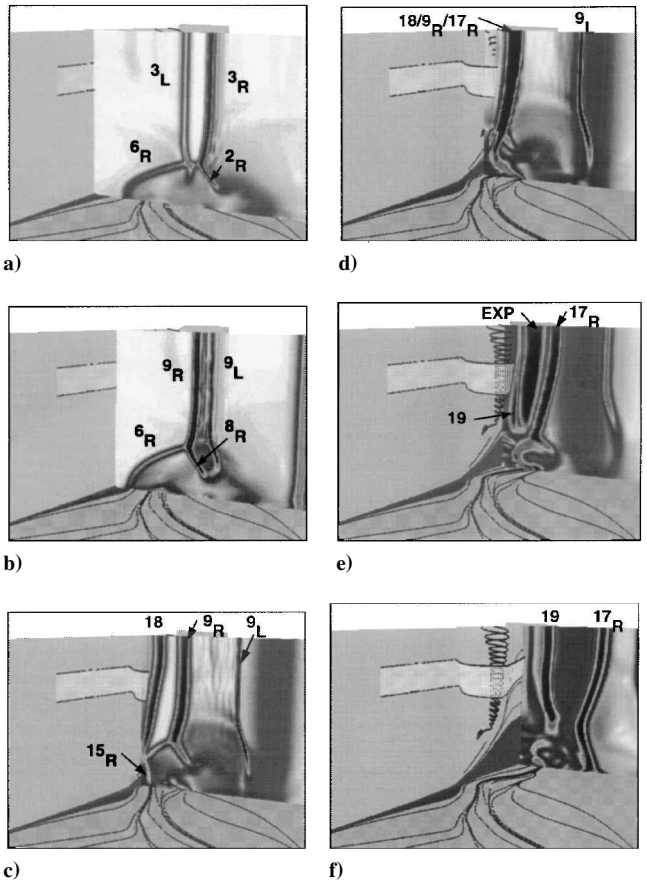

Fig. 11 Shock structure at selected cutting planes.

surface, 15_R interacts in a complicated manner with the secondary vortices noted earlier. Details of this interaction have been described in Ref. 6. The fin boundary-layer recompression shock, 19, and the tertiary inviscid shock, 17_R, straddle the expansion region, as shown in Fig. 11e. The curved shock marked 12, designated as the wall-jet shock because it arises as a result of the stagnation of a wall-jet-like structure,[5] is prominent at this station. Finally, the pattern downstream of the line of attachment R_5 is plotted in Fig. 11f. At this station, the expansion is relatively weaker than at upstream stations, and the recompression shock is much better defined. The tertiary shock system gradually ceases to resemble a λ shock as it encounters the more uniform flow away from the sidewall, similar to the effect described in Ref. 5 in the context of symmetric interactions.

Conclusions

The phenomena arising as a result of the impingement of a crossing-shock-induced vortical structure on a sidewall have been examined numerically. This interaction is shown to be sensitive to the nature of the sidewall boundary layer. A relatively straightforward modification to the baseline k–ϵ model is employed to inhibit the artifically large production of turbulence energy through the leading-edge shock. This strategy yields better agreement between simulated and experimental sidewall oil flow patterns. The topological observations include three-dimensional features consistent with separation of the sidewall boundary layer and attachment of fluid from the region near the fin–plate corner. A prominent focus is shown to correlate with the ejection of the corner vortex along the sidewall in a direction normal to the flat plate. The streamline structure is correlated with other aspects of the flowfield, with particular emphasis on the shock structure in the vicinity of the sidewall interaction.

Acknowledgments

The support of several agencies is gratefully acknowledged. Authors based in the United States were supported by the Air Force Office of Scientific Research (monitors: S. Walker and R. Canfield) and by the Major Shared Resource Centers at Corps of Engineers, Waterways Engineering Station, Naval Oceanographic Office, and Aeronautical Systems Center. Authors affiliated with Institute of Theoretical and Applied Mechanics were supported by the Russian Foundation for Basic Research (Project Codes 96-01-01777 and 97-01-00885) and European Office of Aerospace Research and Development (monitor: C. Raffoul).

References

[1]Panaras, A. G., "Review of the Physics of Swept-Shock/Boundary Layer Interactions," *Progress in Aerospace Sciences*, Vol. 31, 1995, pp. 173–244.

[2]Settles, G. S., and Dolling, D. S., "Swept Shock/Boundary-Layer Interactions: Tutorial and Update," AIAA Paper 90-0375, Jan. 1990.

[3]Zheltovodov, A., Maksimov, A., Shevchenko, A., Vorontsov, S., and Knight, D., "Experimental Study and Computational Comparison of Crossing Shock Wave-Turbulent Boundary Layer Interaction," *International Conference on Methods of Aerophysical Research*, Inst. of Theoretical and Applied Mechanics, Russian Academy of Sciences, Novosibirsk, Russia, Aug. 1994.

[4]Gaitonde, D., Shang, J. S., and Visbal, M. R., "Structure of a Double-Fin Turbulent Interaction at High Speed," *AIAA Journal*, Vol. 33, No. 2, 1995, pp. 193–200.

[5]Gaitonde, D., and Shang, J. S., "The Structure of a Double-Fin Turbulent Interaction at Mach 4," *AIAA Journal*, Vol. 33, No. 12, 1995, pp. 2250–2258.

[6]Gaitonde, D., Shang, J. S., Garrison, T. J., Zheltovodov, A. A., and Maksimov, A. I., "Three-Dimensional Turbulent Interactions Caused by Asymmetric Crossing-Shock Configurations," *AIAA Journal*, Vol. 37, No. 12, 1999, pp. 1602–1608.

[7]Anderson, D. A., Tannehill, J. C., and Pletcher, R. H., *Computational Fluid Mechanics and Heat Transfer*, McGraw–Hill, New York, 1984.

[8]Roe, P. L., "Approximate Riemann Solvers, Parameter Vectors and Difference Schemes," *Journal of Computational Physics*, Vol. 43, No. 2, 1981, pp. 357–372.

[9]Jones, W. P., and Launder, B. E., "The Prediction of Laminarization with a Two-Equation Model of Turbulence," *International Journal of Heat and Mass Transfer*, Vol. 15, No. 2, 1972, pp. 301–314.

[10]Launder, B. E., and Sharma, B. I., "Application of the Energy Dissipation Model of Turbulence to the Calculation of Flows Near a Spinning Disk," *Letters in Heat and Mass Transfer*, Vol. 1, 1974, pp. 131–138.

[11]Sarkar, S., Erlebacher, G., Hussaini, M. Y., and Kreiss, H. O., "The Analysis and Modelling of Dilational Terms in Compressible Turbulence," *Journal of Fluid Mechanics*, Vol. 227, 1991, pp. 473–493.

[12]Visbal, M. R., "Structure of Laminar Juncture Flows," *AIAA Journal*, Vol. 29, No. 8, 1991, pp. 1273–1282.

[13]Rizzetta, D. P., "Numerical Investigation of Supersonic Wing-Tip Vortices," AIAA Paper 95-2282, June 1995.

[14]Gaitonde, D., Edwards, J. R., and Shang, J. S., "The Computed Structure of a 3-D Turbulent Interaction Caused by a Cylinder/Offset Flare Juncture," AIAA Paper 95-0230, Jan. 1995.

[15]Knight, D. D., and Degrez, G., "Shock Wave Boundary Layer Interactions in High Mach Number Flows—A Critical Survey of Current CFD Prediction Capabilities," TR AR-319, Vol. 2, AGARD, 1997.

[16]Gaitonde, D. V., and Shang, J. S., "On 3-D Shock-Wave/Turbulent Boundary Layer Interactions at Mach 4," AIAA Paper 96-0043, Jan. 1996.

[17]Gaitonde, D., and Shang, J. S., "Skin-Friction Predictions in a Crossing-Shock Turbulent Interaction," *Journal of Propulsion and Power*, Vol. 13, No. 3, 1997, pp. 342–348.

[18]Settles, G. S., Vas, I. E., and Bogdonoff, S. M., "Details of a Shock-Separated Turbulent Boundary Layer at a Compression Corner," *AIAA Journal*, Vol. 14, No. 12, 1976, pp. 1709–1715.

[19]Tobak, M., and Peake, D. J., "Topology of Three-Dimensional Separated Flows," *Annual Review of Fluid Mechanics*, Vol. 14, 1982, pp. 61–85.

[20]Chapman, G. T., and Yates, L. A., "Topology of Flow Separation on Three-Dimensional Bodies," *Applied Mechanics Reviews*, Vol. 44, No. 7, 1991, pp. 329–345.

[21]Menter, F. R., "Zonal Two Equation k–w Turbulence Models for Aerodynamic Flows," AIAA Paper 93-2906, July 1993.

[22]Knight, D., Horstman, C., Shapey, B., and Bogdonoff, S., "Structure of Supersonic Turbulent Flow Past a Sharp Fin," *AIAA Journal*, Vol. 25, No. 10, 1987, pp. 1331–1337.

[23]Garrison, T. J., and Settles, G. S., "Flowfield Visualization of Crossing Shock-Wave/Boundary Layer Interactions," AIAA Paper 92-0750, Jan. 1992.

[24]Henderson, L. F., "The Reflexion of a Shock Wave at a Rigid Wall in the Presence of a Boundary Layer," *Journal of Fluid Mechanics*, Vol. 30, No. 4, 1967, pp. 699–722.